Development of daily PM_{10} and $PM_{2.5}$ prediction system using a deep long short-term memory neural network model

Hyun S. Kim[1,†], Inyoung Park[2,†], Chul H. Song[1], Kyunghwa Lee[1], Jae W. Yun[2], Hong K. Kim[2], Moongu Jeon[2], Jiwon Lee[2], Kyung M. Han[1]

[1]School of Earth Sciences and Environmental Engineering, Gwangju Institute of Science and Technology (GIST), Gwangju 61005, Korea
[2]School of Electrical Engineering and Computer Science, Gwangju Institute of Science and Technology (GIST), Gwangju 61005, Korea
[†]Both authors are equally contributed to this work

Correspondence to: Chul Han Song (chsong@gist.ac.kr)

Abstract. A deep recurrent neural network system based on a long short-term memory (LSTM) model was developed for daily PM_{10} and $PM_{2.5}$ predictions in South Korea. The structural and learnable parameters of the newly developed system were optimized from iterative model trainings. Independent variables were obtained from ground-based observations over 2.3 years. The performance of the particulate matter (PM) prediction LSTM was then evaluated by comparisons with ground PM observations and with the PM concentrations predicted from two sets of 3-D chemistry-transport model (CTM) simulations (with and without data assimilation for initial conditions). The comparisons showed, in general, better performance with the LSTM than with the 3-D CTM simulations. For example, in terms of IOAs (index of agreements), the PM prediction IOAs were enhanced from 0.36-0.78 with the 3-D CTM simulations to 0.62-0.79 with the LSTM-based model. The deep LSTM-based PM prediction system developed at observation sites is expected to be further integrated with 3-D CTM-based prediction systems in the future. In addition to this, further possible applications of the deep LSTM-based system are discussed, together with some limitations of the current system.

1 Introduction

Over the past several decades, South Korea has made continuous economic growth; however, in accordance with this rapid economic development, emissions of air pollutants from various sources such as industrial, transportation, and power generation sectors have increased, and air quality has thus deteriorated (Wang et al., 2014). Among the atmospheric pollutants, particulate matter (PM) plays an important role in human health and climate change (Davidson et al., 2005; Forster et al., 2007). Several epidemiological studies have reported clear statistical relationships between aerosol concentrations and human mortality and morbidity (Dockery et al., 1992; Hope III and Dockery, 2006). To minimize the public damage caused by air pollution and to alert Korean citizen about high PM events, the National Institute of

Environmental Research (NIER) of South Korea has carried out daily air quality (or chemical weather) forecasting using multiple 3-D chemistry-transport models (CTMs) since 2014.

However, the accuracy of the 3-D CTM simulations has been reported to be low. Researchers believe that this low accuracy originates from uncertain sources of emission inventory, meteorological fields, initial and boundary conditions, and CTMs themselves (Seaman, 2000; Berge et al., 2001; Liu et al., 2001; Holloway et al., 2008; Tang et al., 2009; Han et al., 2011). Many efforts have been made to enhance the accuracy of the 3-D CTM-based forecasting system. As a part of the efforts, the Korean government decided to develop its own air quality forecasting system mainly based on a new CTM in 2017. This project entailed establishing better bottom-up and top-down emissions, developing improved meteorological fields over East Asia, developing a data assimilation system using satellite-retrieved and ground-based observations, and incorporating new atmospheric chemical/physical processes into the new Korean CTM. Despite all the ongoing efforts, the traditional chemical weather forecasts based on the CTM are still poor at conducting accurate air quality forecasts over South Korea.

In contrast, statistical models based on artificial neural networks (ANNs) have also been applied to air quality predictions. Because these approaches are based on a statistical method instead of sophisticated mathematical model-based computations (i.e., without considerations of advection/convection, photochemistry, or emissions), they are more cost-effective than 3-D CTM simulations. In previous studies, simple ANN models were applied to air quality predictions. The time-series concentrations of ambient pollutants have been predicted by, for example, supported vector machine (SVM) and radial basis function (RBF) neural network models (Lu and Wang, 2005). Furthermore, ambient levels of ozone were predicted by a simple feed-forward neural network (FFNN) models (Yi and Rybutok, 1996; Abdul-Wahab and Al-Alawi, 2002). However, such simple models have the limitation of neglecting relationships among data at the different time steps. Recently, more complex ANN models have been developed with recurrent neural networks (RNNs). Although RNNs have typically been used for natural language recognition, they have the special advantage of remembering the experiences of past events because they maintain the activated vectors at each time step (Cho et al., 2014). Because of this advantage, RNNs also make accurate time-series predictions (Che et al., 2018). Several investigators used a shallow (single hidden layer) RNN model to predict the peak mixing ratios of ambient pollutants such as NO_2, SO_2, O_3, CO, and PM_{10} (Brunelli et al., 2007), and others used a deep RNN model to predict ambient levels of $PM_{2.5}$ (Ong et al., 2016). However, RNN models have generally shown serious exploding and/or vanishing gradient problems (Bengio et al., 1994; Hochreiter, 1998). To resolve these problems, researchers developed the long short-term memory (LSTM) cell (Hochreiter and Schmidhuber, 1997). Unlike traditional RNNs, LSTM is known to be free from exploding or vanishing gradient problems, and it is better suited for long time-series predictions than are traditional RNNs. Recently, researchers used a deep LSTM neural network to conduct a number of air quality studies (Li et al., 2017; Freeman et al., 2018).

Although ANN-based predictions are not mathematics-based, deep learning has demonstrated strong potential in the areas of weather and air quality forecasts; for example, the Weather Channel in the United States uses IBM Watson for its operational weather predictions (Mourdoukoutas, 2015). Another example is bias corrections based on several machine-learning techniques. Authors of one study reported that the biases (or errors) between the operational CTM-based air quality

predictions and observations can be reduced by utilizing machine learning algorithms (Reid et al., 2015). There must be many creative ways to improve the accuracy of air quality forecasts by combining 3D CTM-based predictions with artificial intelligence (AI)-based techniques. These combined approaches have now begun, and this manuscript intends to present one of these efforts in the area of air quality predictions.

5   For this study, we developed a deep LSTM model to more accurately predict ambient PM concentrations. We evaluated the model performance by comparing the CTM-predicted and observed PM_{10} and $PM_{2.5}$ with the LSTM-predicted PM_{10} and $PM_{2.5}$. The details of the system development and prediction procedures are presented in Sects. 2 and 3, and limitations of the model are discussed in Sect. 4.

2 Model development

10   Fig. 1 shows the schematic procedures for the deep LSTM model-based PM predictions. There were two main processes in developing this prediction system: (i) data preprocessing and (ii) structure design and optimization of the deep neural network. It is essential to prepare time-series sequential data sets for both model training and predictions. In this study, we collected ambient pollutant concentrations and meteorological data from ground-based observations. To construct the system, we first screened several AI-based methods including LSTM, such as SVM, relevance vector machine (RVM), and a

15   technique from convolutional neural network (CNN). Based on the results from the screening, we chose a multi-layered deep LSTM neural network and conducted iterative model training to optimize the weights and biases of models at 7 individual site. We present the details on developing the system in the following sections.

2.1 Data preprocessing

We collected the observation data from both the NIER AIR KOREA measurement network and the Korea Metrological

20   Administration (KMA) automatic weather station (AWS) network to prepare the input variables. Fig. 2 presents the locations of the AIR KOREA and KMA AWS observation sites throughout South Korea; the networks consist of 323 and 494 ground-based monitoring stations, respectively. They provide hourly mixing ratios of the ambient pollutants such as SO_2, CO, NO_2, O_3, PM_{10}, and $PM_{2.5}$ and the metrological parameters such as temperature, wind direction, wind speed, hourly precipitation, and relative humidity. Both PM_{10} and $PM_{2.5}$ are measured by β-ray absorption and gravimetric method, respectively (Shin et

25   al., 2011). The ambient mixing ratios of SO_2, CO, NO_2, and O_3 are measured by pulse ultraviolet fluorescence, non-dispersive infrared, chemiluminescence, and ultraviolet methods, respectively.

Among the observation sites, we chose seven monitoring sites located in the major cities in South Korea (two sites in Seoul, Daejeon, Gwangju, Daegu, Ulsan, and Busan) for PM_{10} and $PM_{2.5}$ predictions (refer to Fig. 2 (a)-(f) regarding the locations). There were two main criteria in our selecting the seven sites: (i) the distances between air quality and meteorological

30   monitoring stations should be the shortest (i.e., collocation), and (ii) the number of missing observation data should be minimal. Because there are sometimes too many missing values in the monitoring data prior to 2013, we used observations

3

from January 2014 to April 2016 for training. After the model training, actual predictions of PM_{10} and $PM_{2.5}$ were conducted for the period of the Korea-United States Air Quality (KORUS-AQ) campaign (from May 1 to June 11, 2016). The KORUS-AQ campaign period is now an official model testing window in South Korea.

High quality of input data is critical for LSTM-based time-series predictions. In the current study, the missing values in ground-based air quality monitoring data were produced by using the pre-trained deep LSTM model. The percentages of missing observations at the seven AIR KOREA sites are summarized in Table S1. The percentage ranged between 0.7 % and 13.9 %. The schematic diagram of missing value generation is presented in Fig. S1. As shown in Fig. S1, when the missing data were detected, the corresponding values were generated from a pre-trained model. For example, the accuracy of the missing values generated for Seoul-1 site is summarized in Fig. S2. It is shown from Fig. S2 that the pollutant concentrations generated by the pre-trained model correlated well with the observed concentrations. The correlation coefficients for the model training and validation ranged from 0.60 to 0.91 and from 0.52 to 0.93, respectively. The accuracy of the generated missing values from the seven selected monitoring stations is summarized in Table S2. For the meteorological parameters, we determined the missing variables by interpolating the observed data; in the meteorological data, fewer than 0.01 % of values were missing.

In particular, information on various pollutants is important in the LSTM-based predictions of PM_{10} and $PM_{2.5}$. Because H_2SO_4 and HNO_3 are main precursors of inorganic sulfate (SO_4^{2-}) and nitrate (NO_3^-), respectively, correct information on the levels of their precursors (SO_2 and NO_2) is important. Although CO is not directly related to producing particulate matter, we included the mixing ratios in the input data because these are somehow related to the mixing ratios of ozone and hydroxyl radicals (OH).

Meteorological conditions also play an important role in particulate matter concentrations. Both wind direction and speed can represent the origin of air pollutants and intensity of atmospheric turbulences, and precipitation directly affects PM_{10} and $PM_{2.5}$ by wet scavenging. In addition, there is a relationship between relative humidity and the levels of hydroxyl radicals because H_2O is a main precursor of OH. Water vapor can also influence the amounts of particulate water and nucleation rates in the atmosphere. Therefore, all meteorological parameters measured in the AWS monitoring data set can possibly affect PM concentrations, and thus we used them in the LSTM-based prediction system.

Before feeding the input variables into the LSTM system, one important step is data normalization. All the input parameters were re-scaled between 0 and 1:

$$x_{normal,i} = \frac{x_i - x_{min,i}}{x_{max,i} - x_{min,i}} \tag{1}$$

where $x_{normal,i}$ is the normalized values of species i; x_i is the observed value; $x_{max,i}$ and $x_{min,i}$ are the maximum and minimum values of species i, respectively. Because the LSTM system was designed for daily prediction of PM_{10} and $PM_{2.5}$, the normalized observations of the previous day were mapped with the PM concentrations of the next day (i.e., there is a 24-hr time-lag between independent and dependent variables). Thus, the shapes of one unit of training data are 24×11 and/or

4

24×12. This structured data set was then re-shaped as a three-dimensional vector matrix to feed them into the hidden LSTM layers. In addition, we excluded the observation data during the dust event periods in the model training; because these episodes are infrequent, including data on them could have interfered with establishing an accurate PM prediction system (i.e., they can be noisy signals).

2.2 System construction

As mentioned previously, the LSTM has the special advantage of remembering the past experiences. Because of this advantage, the LSTM has a strong capability for identifying highly complex relationship in the sequential data (i.e., the LSTM-based deep neural network has the strong potential in the time-series predictions). In general, the accuracy of the time-series prediction with the deep LSTM model is relatively higher than those with other deep neural networks (Ma et al., 2015; Amarasinghe et al., 2017). Several previous studies have proposed the use of the LSTM for more accurate time-series predictions (e.g. Connor et al., 1994; Saad et al., 1998). Based on this, in this study we used the LSTM cells in the construction of the deep hidden layers of daily PM_{10} and $PM_{2.5}$ prediction model.

The developed system has two schemes: PM_{10} prediction and $PM_{2.5}$ prediction; the prediction model is designed to have three to five hidden LSTM layers; one layer consists of one hundred hidden nodes, and the layers capture sequential temporal information. The last LSTM hidden layer is connected to the output layer, which performs feature mapping between the output vectors from deep hidden layers and the actual PM_{10} and/or $PM_{2.5}$.

In order to learn complicated and nonlinear mappings between the layers, activation functions are applied to get the output of a layer, which is then fed into the next layer as an input. There are several activation functions that can be used in neural networks; among them, a sigmoid function has been typically used because it has characteristics of being bounded and being differentiable; however, this function has a vanishing gradient problem due to continuous multiplication of gradients. In this study, therefore, we used the rectified linear unit (ReLU) to activate output layer (Nair and Hinton, 2010). The ReLU is expressed by:

$$f(x) = \begin{cases} 0 & when \ x < 0 \\ x & when \ x \geq 0 \end{cases} \tag{2}$$

As shown in Eq. (2), the ReLU ranges from 0 to ∞. Because the derivative of the ReLU is 0 or 1, the vanishing gradient does not occur during the back propagations. In Supplementary Material (SM), we give a detailed description of the LSTM architecture used in this study.

In traditional statistics, the close relationship among the input variables (i.e., multicollinearity) can lead to instability of regression coefficients and can distort the effect of the regressive variables on dependent variables. For the deep learning, the multicollinearity requires relative long computation time, because it is slow to converge. We evaluated the multicollinearity of the independent variables by estimating the Pearson correlation coefficient (R) between the observed atmospheric pollutants at the different time steps because the purpose of recurrent neural network is to identify the relationships in

sequential data. The correlation coefficients are summarized in Table S3; as shown in Table S3, there are relatively low correlations among the concentrations of atmospheric pollutants. In addition, the LSTM-based deep neural network is effective for analyzing the relationships between highly correlated time-series sequential data (Fan et al., 2014). Furthermore, the problem of the multicollinearity can be resolved by adopting ReLU as an activation function (Ayinde et al., 2019).

2.3 Model training

The model training is a process for optimizing the structural and learnable parameters of the deep LSTM system; we determined the PM_{10} and $PM_{2.5}$ prediction system's structure from the iterative trainings, and the structure was described in Sect. 2.2. In addition to the activation functions described in Sect. 2.2, there are two more main components in the deep neural network training: (i) cost function and (ii) optimization algorithm. The cost function usually measures how well the neural network works with respect to given training samples and corresponding predicted outputs. In other words, it is used for evaluating the accuracy of predicted values. When the prediction accuracy is poor, the cost is high, whereas as the model's predictions are more accurate, the cost decreases.

There are several cost functions commonly used in deep learning, and the cost function can be classified by its application purpose. In this study, the purpose of the cost function was to minimize the regression cost, and we thus used mean squared error (MSE) as a cost function, expressed as:

$$J_{MSE}(\theta) = \frac{1}{N}\sum_{i=1}^{N}(y_i - h_\theta(x_i))^2 \tag{3}$$

where x_i is the input vector for i^{th} training; y_i is the target value (or true value) for the ith training; and $h_\theta(x_i)$ is the predicted vector corresponding to y_i for a given deep neural network model θ. It should be noted here that θ means the LSTM network with different parameters (see Eqs. (S1)-(S6) in SM). In Eq. (3), $J_{MSE}(\theta)$ represents the MSE between the target vector, y_i, and its predicted vector, $h_\theta(x_i)$, when the number of training vectors is N.

The role of an optimization algorithm is to find an efficient and stable pathway for minimizing the gradient descent of a cost function. In this study, we utilized adaptive moment estimation (ADAM) to train the neural networks (Kingma and Ba, 2015). The ADAM is one of the extended algorithms for stochastic gradient descent, and its detailed explanation is also given in SM.

In order to train the LSTM system for the PM_{10} and $PM_{2.5}$ predictions, the observations from January 2014 to April 2016 (2.3-year data) were used, as mentioned previously. Because Asian dust was regarded as noisy atmospheric signals, we removed the observations during dust events in the course of the model training. We divided the training data set into two groups with ratios of 0.85 to 0.15 for the model training and validation, respectively (Guyon, 1997).

First, we measured the variations of training and validation costs (i.e., the outcome of MSE cost) during the model training. In the early stages of the model training, updating the weights and biases decreases the training and validation costs. Because

the training data set is only considered for updating weights and biases, the training cost is smaller than the validation cost. With the same reason, the training cost continues to decrease during the model training. In contrast, the validation cost decreases until the certain point of iterations, and then it starts to increase. Optimization of the deep neural network model is to update the weight and bias vectors until the validation cost reaches such inflection point (Mahsereci et al., 2017). In addition, the model training can also be verified by comparing two statistical parameters, MSE and root mean squared error (RMSE); these values at the inflection point are summarized in Table 1. For properly-trained models, the training cost should be slightly smaller than the validation cost. If the validation cost is much higher than training cost and the slope of validation cost is positive, it is called "over-fitting", which means that both the weight and bias vectors of the model have been overturned. Based on the above two essential requirements of the model training, we concluded that our LSTM PM prediction model was well trained via general rules of the model training (refer to Table 1).

Second, the accuracy of the deep LSTM model training for PM_{10} and $PM_{2.5}$ predictions is summarized in Figs. 3 and 4, respectively; in the figures, the black and red dots denote the comparison results between the predicted and observed PM concentrations in the model training and validation, respectively. As shown in Fig. 3, there was reasonable agreement in the PM_{10} predictions. The R for PM_{10} training and validation ranged from 0.61 to 0.81 and from 0.55 to 0.71, respectively. The training results for the $PM_{2.5}$ model also showed reasonable correlations ($0.59 \leq$ R for training ≤ 0.80; $0.54 \leq$ R for validation ≤ 0.75).

2.4 3-D CTM simulations

In order to assess the accuracy of the LSTM-based predictions in this study, we compared them with 3-D CTM-based predictions with and without data assimilation (DA). We employed the Community Multiscale Air Quality (CMAQ) model v5.1 for the 3-D CTM simulations. We acquired the metrological fields from Weather Research and Forecasting v3.8.1 model simulations. The domain of the CMAQ model simulations is presented in Fig. 5; the model domain covers Northeast Asia with a horizontal resolution of 15×15 km^2 and with 27 sigma vertical levels. We used the KORUS v1.0 emission inventory for anthropogenic emissions; this inventory was made for the KORUS-AQ campaign based on three emission inventories: (i) CREATE (Comprehensive Regional Emission inventory for Atmospheric Transport Experiment); (ii) MICS-Asia (Model Inter-Comparison Study for Asia); and (iii) SEAC4RS (Studies of Emissions and Atmospheric Composition, Clouds, and Climate Coupling by Regional Surveys) (Woo et al., 2017). We estimated biogenic emissions from MEGAN v2.1 (Model of Emissions of Gases and Aerosols from Nature) simulations (Guenther et al., 2006). We obtained biomass burning emissions from FINN (Fire INventory from NCAR, http://bai.acom.ucar.edu/Data/fire/) (Wiedinmyer et al., 2011). We obtained lateral boundary conditions from the MOZART-4 model simulations (https://www.acom.ucar.edu/wrf-chem/mozart.shtml) (Emmons et al., 2010).

To prepare the initial conditions (ICs) for the CMAQ model simulations, we used optimal interpolation method with Kalman filter (OI with Kalman). The DA with the OI technique has been used in several previous studies (Carmichael et al., 2009; Chung et al., 2010). The assimilation system is defined as follows:

$$\tau'_m = \tau_m + K\left(\tau_o - H\tau_m\right) \tag{4}$$

$$K = BH^T\left(HBH^T - O\right)^{-1} \tag{5}$$

where τ'_m represents the assimilated product; τ_o and τ_m denote the observed and modeled values, respectively; H represents the observation and/or forward operator; K represents the Kalman gain matrix; and B and O are the covariance of modeled and observed field, respectively. B and O can be defined with several free parameters.

$$B(d_x, d_z) = \left[(f_m \tau_m)^2 + (\varepsilon_m)^2\right]\exp\left[-\frac{d_x^2}{2l_{mx}^2}\right]\exp\left[-\frac{d_z^2}{2l_{mz}^2}\right] \tag{6}$$

$$O = \left[(f_o \tau_o)^2 + (\varepsilon_o)^2\right]I \tag{7}$$

where f_m, ε_m, d_x, d_z, l_{mx}, and l_{mz} represent the fractional error coefficient, minimum error coefficient, horizontal resolution, vertical resolution, horizontal correlation length for errors in modeled values, and vertical correlation length for errors in modeled values, respectively, and f_o, ε_o, and I denote the fractional error coefficient, minimum error coefficient in the observed values, and unit matrix, also respectively. The six parameters in Eq. (6) are called the free parameters, which we used to calculate the observation and model error covariance matrix, respectively. In this study, we determined these parameters by finding the minimum of χ^2:

$$\chi^2 = \sum \frac{(x_{obs} - x_{assim})^2}{x_{assim}} \tag{8}$$

here x_{obs} and x_{assim} represent the observed and data-assimilated values. More detailed explanations regarding the data assimilation can be found elsewhere (Collins et al., 2001; Yu et al., 2003; Park et al., 2011).

For the DA runs, we integrated the CMAQ model simulations with three observation data sets: (i) the Communication, Ocean, and Meteorological Satellite (COMS)/Geostationary Ocean Color Imager (GOCI) aerosol optical depth (AOD); (ii) ground-based observations in China; and (iii) AIR KOREA observations in South Korea. The locations of the observation stations are presented in Fig. 5. Because the GOCI sensor is geostationary, it can provide hourly spectral images with spatial resolution of 500×500 m^2 from 00:00 to 07:00 UTC. Detailed procedures can also be found in previous publications (Park et al., 2014; Park et al., 2014).

3 Results and Discussion

PM_{10} and $PM_{2.5}$ were predicted for the period of the KORUS-AQ campaign. To evaluate the performance of the LSTM system, we compared the LSTM-based predictions with the observations and two CMAQ-based predictions.

3.1 System evaluation

We evaluated the accuracy of the LSTM-based PM predictions by comparing them with the observed PM_{10} and $PM_{2.5}$. We also compared PM_{10} and $PM_{2.5}$ predicted from two sets of CMAQ model simulations with the PM_{10} and $PM_{2.5}$ predicted from the deep LSTM; these results are presented in Figs. 6 and 7. In Figs. 6 and 7, the black circles and blue-dashed lines

5   represent the observed and LSTM-predicted PM_{10} and $PM_{2.5}$, respectively. The green- and red-dashed lines denote CMAQ-predicted PM_{10} and $PM_{2.5}$ with and without DA, respectively. The CMAQ model simulations with DA showed better agreement with the observations than did those without DA (see Figs. 6 and 7). The LSTM-predicted PM_{10} also showed good agreement with the observed PM_{10}.

However, the results from the CMAQ model simulations were not intended to be directly compared with those from the

10   LSTM predictions. In general, Eulerian CTMs calculate average concentrations of air pollutants in a grid box, but in the real world the concentrations of air pollutants inside a gird box can be (highly) variable with the proximity to the local sources (in other words, the air pollutant concentrations in a gird box cannot be uniform). This is well-known problem called "sub-grid variability". In this sense, both the CMAQ-model results and LSTM predictions were not directly compared. Instead, in this comparison the CMAQ model simulations provide reference values to give a sense for the accuracy of LSTM

15   predictions. An intension to develop the LSTM prediction system is to establish a prediction system at the observation sites (i.e., point site), and we then eventually plan to integrate the CTM-LSTM prediction (gird-based prediction and point-based prediction) system for more comprehensive PM forecasting in South Korea. This will be discussed further in Sect. 4.

For further statistical evaluations, we introduced the following five statistical parameters: (i) IOA; (ii) RMSE; (iii) MB (Mean Bias); (iv) MNGE (Mean Normalized Gross Error); and (v) MNB (Mean Normalized Bias).

20   $$IOA = 1 - \frac{\sum_{1}^{N}\left(C_{i,Model} - C_{i,Obs}\right)^2}{\sum_{1}^{N}\left(\left|C_{i,Model} - \overline{C_{i,Obs}}\right| + \left|C_{i,Obs} - \overline{C_{i,Obs}}\right|\right)^2} \tag{9}$$

$$RMSE = \sqrt{\frac{1}{N}\sum_{1}^{N}\left(C_{i,Model} - C_{i,Obs}\right)^2} \tag{10}$$

$$MB = \frac{1}{N}\sum_{1}^{N}\left(C_{i,Model} - C_{i,Obs}\right) \tag{11}$$

$$MNGE = \frac{1}{N}\sum_{1}^{N}\left(\frac{\left|C_{i,Model} - C_{i,Obs}\right|}{C_{i,Obs}}\right) \times 100 \tag{12}$$

9

$$MNB = \frac{1}{N} \sum_1^N \left(\frac{C_{i,Model} - C_{i,Obs}}{C_{i,Obs}} \right) \times 100 \qquad (13)$$

Here, $C_{i,Model}$ and $C_{i,Obs}$ represent the modeled and observed concentrations of species i; $\overline{C_{i,Obs}}$ is the averaged $C_{i,Obs}$. The results from the statistical analysis are summarized in Table 2 and are also shown in Figs. 6 and 7.

For the daily PM_{10} predictions, the LSTM-based predictions ($0.62 \leq IOA \leq 0.79$) were always more accurate than two CMAQ-based PM_{10} predictions ($0.36 \leq IOA \leq 0.78$). RMSE and MB between the CMAQ-based and observed PM_{10} ranged between 33.11 μg/m^3 and 51.40 μg/m^3 and between -40.35 μg/m^3 and -15.95 μg/m^3, respectively. These negative MBs indicate that the CMAQ model simulations underestimated PM_{10}. RMSE and MB between the LSTM-based predictions and observations ranged from 18.57 μg/m^3 to 24.23 μg/m^3 and from -3.20 μg/m^3 to 6.28 μg/m^3, respectively. The RMSEs for the LSTM-based predictions are 1.90 times smaller than those for the CMAQ-based predictions. Among the seven sites chosen, the PM_{10} predictions at the Daegu, Ulsan, and Busan sites showed the best agreement ($0.71 \leq IOA \leq 0.79$) and the lowest errors and biases ($16.46 \leq RMSE \leq 18.57$; $-1.00 \leq MB \leq 6.02$) compared with the two CMAQ-based PM_{10} predictions ($0.45 \leq IOA \leq 0.65$; $26.23 \leq RMSE \leq 55.09$; $-37.69 \leq MB \leq -15.92$).

Fig. 7 presents the comparisons for $PM_{2.5}$. During the KORUS-AQ campaign, there were no ground $PM_{2.5}$ observations at the Daejeon site between May 1 and June 11 because of instrument malfunction. The LSTM-predicted $PM_{2.5}$ again showed good agreement with the observations ($0.63 \leq IOA \leq 0.79$); however, the deep LSTM system was not always able to more accurately predict $PM_{2.5}$. As with PM_{10}, the LSTM $PM_{2.5}$ predictions at the Daegu, Ulsan, and Busan sites showed better performance ($0.78 \leq IOA \leq 0.79$) than the CMAQ-based predictions ($0.59 \leq IOA \leq 0.75$), but at the two Seoul sites (Seoul-1 and Seoul-2), the LSTM $PM_{2.5}$ predictions were inferior to those from the CMAQ model simulations with DA (green-dashed lines in Fig. 7). This could have been because the AIR KOREA observation sites are densely located in and around Seoul Metropolitan Area (refer to Fig. 2). Therefore, data assimilation appears to more strongly influence the accuracy of the CMAQ predictions.

As shown in Figs. 6 and 7, there were nationwide high PM episodes from May 25 to 28, 2016; these high PM events were caused by long-distance transport of atmospheric pollutants from China due to westerlies, and the relatively high errors and biases in the LSTM-based predictions occurred during these high PM events. Because the model's weights and biases were optimized based on previous memories, frequent high PM episodes can affect the accuracy of the predictions. The frequencies of the high PM_{10} (daily average of $PM_{10} \geq 70$ μg/m^3) and high $PM_{2.5}$ (daily average of $PM_{2.5} \geq 40$ μg/m^3) episodes in the training data set are summarized in Fig. 8. The fractions of the high $PM_{2.5}$ episodes at the Seoul and Gwangju sites were between 0.04 and 0.09, clearly smaller than those at Daegu, Ulsan, and Busan ($0.12 \leq$ high $PM_{2.5}$ episode ≤ 0.18). At Gwangju, the effectiveness of DA and frequency of high PM episodes were the lowest. As mentioned previously, the LSTM-based PM_{10} and $PM_{2.5}$ prediction system was trained using the observation data for only 2.3 years because these were the only available data. The optimized weights and biases are governed by the variety of input features in the training. If

more $PM_{2.5}$ data are available in the future, the prediction accuracy of deep LSTM systems will improve, and in fact, continuous data accumulation with more recent PM data is now underway.

Imbalance of the training data set has deteriorated the performances of the deep neural network model. As shown in Fig. 8, the frequency of high PM_{10} and $PM_{2.5}$ events is very low. There are a number of ways to balance data, such as minority oversampling and majority subsampling. The prerequisite for the data balancing is that the amounts of available data should be very large. As mentioned previously, the AIR KOREA network has monitored ground $PM_{2.5}$ only since 2015. Therefore, the amount of available data is relatively small, and compulsory data balancing is highly likely to hinder the generalization of the PM prediction model. Therefore, we did not perform the data balancing in this study.

To test the effectiveness of the data balancing, we did balance the data for the observations of Seoul-1 site; at this site, the CMAQ-based $PM_{2.5}$ predictions were better than the LSTM-based $PM_{2.5}$ predictions. Because of the data availability, it was impossible to balance the training data set with subsampling method, and thus we oversampled atmospheric conditions during the high $PM_{2.5}$ events. To balance the numbers of high and non-high events, we replicated the ground observations during the high $PM_{2.5}$ events; then we generated ±5% Gaussian random noise on these oversampled data to reflect the observational errors. The $PM_{2.5}$ predictions with and without the data balancing are represented in Fig. S4. As shown in Fig. S4, the data balancing did not improve the prediction performances of the LSTM model. This is because we could not sample the various types of high $PM_{2.5}$ events, and similar patterns of atmospheric conditions were consistently considered in the model training. Therefore, to improve the performances of the LSTM-based PM prediction model, it is necessary to collect various atmospheric conditions through continuous ground-based observations.

3.2 Dependence on input parameters

In deep learning, the relationships between input variables and predictions cannot be identified directly because of the high non-linearity in the hidden layers. In the present study, we indirectly investigated the influences of the input parameters on the PM_{10} and $PM_{2.5}$ predictions with and without considering each variable in the model operations. The influences on the input parameters are summarized in Figs. 9 and 10; in the figures, TA, WD, WS, RN, RNH, and RH represent temperature, wind direction, wind speed, daily cumulative precipitation, hourly precipitation, and relative humidity on the previous day, respectively. SO_2, O_3, NO_2, CO, PM_{10}, and $PM_{2.5}$ are the concentrations of the respective air pollutants on the previous day. The positive and negative values in each figure represent the directionality of the influences on the PM_{10} and $PM_{2.5}$ predictions; that is, for instance, the variables with positive dependence indicate increasing influence on the predicted PM_{10} and $PM_{2.5}$. The figures show that among the meteorological variables, temperature and wind direction generally had great influence on the PM_{10} and $PM_{2.5}$ predictions; among the pollutant variables, previous day's PM_{10} and $PM_{2.5}$ mainly affected the predictions for the next day. In particular, the dependencies of PM_{10} and $PM_{2.5}$ ranged from 38.48 % to 60.12 % and from 28.80 % to 83.38 %, respectively. In most cases, the influence of the pollutant variables (PM_{10} and $PM_{2.5}$) was greater than that of the meteorological parameters. However, at Daejeon, the most influential parameter on the PM_{10} predictions was wind direction (45.67 %), while the contributions of other parameters were relatively small. The difference in the

11

contributions is mainly due to the persistence of each variable. In other words, the variables with low dependence on the PM_{10} and $PM_{2.5}$ predictions were those that change rapidly in the atmosphere, and thus their effects are scarcely incorporated into the trained model.

4 Outlook and future works

5 In this study, we established a deep RNN system for daily PM_{10} and $PM_{2.5}$ predictions and evaluated the newly developed system's performance by comparing its PM_{10} and $PM_{2.5}$ predictions with the observed and CMAQ-predicted levels. In the comparisons, the LSTM-based PM predictions were, in general, superior to the CMAQ-based PM predictions. In terms of IOA, the accuracies of the LSTM predictions were 1.01-1.72 times higher than those for the CMAQ-based predictions. Based on this, we concluded that the LSTM-based system could be applied to daily "operational" PM_{10} and $PM_{2.5}$ forecasts.

10 The LSTM-based predictions at the observation sites can provide useful and complementary information for air quality forecasters, synthesizing all the information available such as CTM air quality predictions, AI predictions, weather predictions, and satellite-derived information.

In the future, Korea's air quality forecasting system will be improved by continuous development of CTM-based prediction system including the uses of more advanced DA techniques, together with continuous sophistication of AI-based prediction

15 system. If the AI-based predictions at the observation sites are consistently better than the CTM-based predictions, the two elements will be more systematically combined within a prognostic mode, which will be our final research goal. In addition, a similar LSTM-based prediction system can also be applied to the daily forecasts of gas-phase air pollutants such as NO_2, SO_2, CO, and O_3. These works are also now in progress.

Although the current LSTM-based system can accurately predict PM_{10} and $PM_{2.5}$, it also has some limitations. One, for better

20 prediction accuracy, we need more air quality data for model optimization. Because $PM_{2.5}$ has only been monitored in South Korea since 2015, there are too few observations to optimize the $PM_{2.5}$ predictions, which require continuous accumulation of $PM_{2.5}$ observations. In addition, the limited number of input variables is another obstacle to optimal model performance. The current LSTM-based PM_{10} and $PM_{2.5}$ prediction system contains 10-12 input parameters. If more useful parameters such as mixing layer height (MLH) and barometric distribution are available, its performance would improve further (Hooyberghs

25 et al., 2005; Liu et al., 2007). Therefore, future efforts should be made with more $PM_{2.5}$ data and more input variables such as mixing layer heights entered into our system.

References

Abdul-Wahab, S. A. and Al-Alawi, S. M.: Assessment and prediction of tropospheric ozone concentration levels using artificial neural networks, Environ. Modell. Softw., 17, 219-228, 2002.

Amarasinghe, K., Marino, D. L., and Manic, M: Deep neural networks for energy load forecasting, in: Proceedings of the
5   26th IEEE International Symposium on Industrial Electronics, Scotland, UK, 1483-1488, 2017.

Ayinde, B. O., Inanc, T., and Zurada, J. M.: On Correlation of Features Extracted by Deep Neural Networks, arXiv:1901.10900v1, 2019.

Bengio, Y., Simard, P., and Frasconi, P.: Learning long-term dependencies with gradient descent is difficult, IEEE Trans. Neural Netw., 5,157–166, 1994.

10   Berge, E., Huang, H.-C., Chang, J., and Liu, T.-H.: A study of importance of initial conditions for photochemical oxidant modeling, J. Geophys. Res. Atmos., 106(D1), 1347-1363, 2001.

Brunelli, U., Piazza, V., Pignato, L., Sorbello, F., and Vitabile, S.: Two-days ahead prediction of daily maximum concentrations of SO_2, O_3, PM_{10}, NO_2, CO in the urban area of Palermo, Italy, Atmos. Environ., 41, 2967-2995, 2007.

Carmichael, G. R., Adhikary, B., Kulkarni, S., D'Allura, A., Tang, Y., Streets, D., Zhang, Q., Bond, T. C., Ramanathan, V.,
15   Jamroensan, A., and Marrapu, P.: Asian aerosols: Current and year 2030 distributions and implications to human health and regional climate change, Environ. Sci. Technol., 43, 5811-5817, 2009.

Che, Z., Purushotham, S., Cho, K., Sontag, D., and Liu, Y.: Recurrent neural networks for multivariate time series with missing values, Sci. Rep., 8, DOI:10.1038/s41598-018-24271-9, 2018.

Cho, K., van Merrienboer, B., Gulcehre, C; Bougares, F., Schwenk, H., Bahdanau, D., and Bengio, Y.: Learning phrase
20   representations using rnn encoder-decoder for statistical machine translation, in: Proceedings of the 19th Conference on Empirical Methods in Natural Language Processing, Doha, Qatar, 25-29 October, 1724-1734, 2014.

Chung, C. E., Ramanathan, V., Carmichael, G., Kulkarni, S., Tang, Y., Adhikary, B., Leung, L. R., and Qian, Y.: Anthropogenic aerosol radiative forcing in Asia derived from regional models with atmospheric and aerosol data assimilation, Atmos. Chem. Phys., 10, 6007–6024, 2010.

25   Collins, W. D., Rasch, P. J., Eaton, B. E., Khattatov, B. V., Lamarque, J.-F., and Zender, C. S.: Simulating aerosols using a chemical transport model with assimilation of satellite aerosol retrievals: Methodology for INDOEX, J. Geophys. Res., 106(D7), 7313–7336, 2001.

Connor, J. T., Martin, D., and Atlas, L. E.: Recurrent neural networks and robust time series prediction, IEEE Trans. Neural Netw., 5, 240-253, 1994.

30   Davidson, C. I., Phalen, R. F., and Solomon, P. A.: Airborne particulate matter and human health: A review, Aerosol Sci. Tech., 39, 737–749, 2005.

Dockery, D. W., Schwartz, J., and Spengler, J. D.: Air pollution and daily mortality: associations with particulates and acid aerosols, Environ. Res., 59, 362-373, 1992.

Emmons, L. K., Walters, S., Hess, P. G., Lamarque, J.-F., Pfister, G. G., Fillmore, D., Granier, C., Guenther, A., Kinnison, D., Laepple, T., Orlando, J., Tie, X., Tyndall, G., Wiedinmyer, C., Baughcum, S. L., and Kloster, S.: Description and evaluation of the Model for Ozone and Related chemical Tracers, version 4 (MOZART-4), Geosci. Model Dev., 3, 43–67, 2010.

Fan, Y., Qian, Y., Xie, F.-L., and Soong, F. K.: TTS synthesis with bidirectional LSTM based recurrent neural networks, in: Proceedings of the 15th Annual Conference of the International Speech Communication Association, Singapore, Singapore, 14-18 September, 1964-1968, 2014.

Forster, P., Ramaswamy, V., Artaxo, P., Berntsen, T., Betts, R., Fahey, D. W., Haywood, J., Lean, J., Lowe, D. C., Myhre, G., Nganga, J., Prinn, R., Raga, G., Schulz, M., and Van Dorland, R.: Changes in Atmospheric Constituents and in Radiative Forcing. In Climate Change 2007: The Physical Science Basis, Contribution of Working Group I to the Fourth Assessment Report of the Intergovernmental Panel on Climate Change, edited by: Solomon, S. D. Qin, M. Manning, Z. Chen, M. Marquis, K. B. Averyt, Tignor M., and Miller, H. L., Cambridge University Press: Cambridge, U. K. and New York, 2007.

Ma, X., Tao, Z., Wang, Y., Yu, H., and Wang, Y.: Long short-term memory neural network for traffic speed prediction using remote microwave sensor data. Transp. Res. Part C Emerg. Technol., 54, 187–197, 2015.

Freeman, B. S., Taylor, G., Gharabaghi, B., and Thé, J.: Forecasting air quality time series using deep learning, J. Air Waste Manage. Assoc., 68, 866-886, 2018.

Guenther, A., Karl, T., Harley, P., Wiedinmyer, C., Palmer, P. I., and Geron, C.: Estimates of global terrestrial isoprene emissions using MEGAN (Model of Emissions of Gases and Aerosols from Nature), Atmos. Chem. Phys., 6, 3181–3210, 2006.

Guyon, I.: A scaling law for the validation-set traning-set size ratio, AT&T Bell Laboratories, 1997.

Han, K. M., Lee, C. K., Lee, J., Kim, J., and Song, C. H.: A comparison study between model-predicted and OMI-retrieved tropospheric NO_2 columns over the Korean peninsula, Atmos. Environ., 45, 2962-2971, 2011.

Hochreiter, S. and Schmidhuber, J.: Long short-term memory, Neural Comput., 9, 1735-1780, 1997.

Hochreiter, S.: The vanishing gradient problem during learning recurrent neural nets and problem solutions, Int. J. Uncertainty Fuzziness Knowl.-Based Syst., 6, 107-116, 1998.

Holloway, T., Spak, S. N., Barker, D., Bretl, M., Moberg, C., Hayhoe, K., Van Dorn, J., and Wuebbles, D.: Change in ozone air pollution over Chicago associated with global climate change. J. Geophys. Res. Atmos., 113 (D22306), doi:10.1029/2007JD009775, 2008.

Hope III, C. A. and Dockery, D. W.: Health effects of fine particulate air pollution: lines that connect, J. Air Waste Manage. Assoc., 56, 709-742, 2006.

Hooyberghs, J., Mensink, C., Dumont, G., Fierens, F., and Brasseur, O., A neural network forecast for daily average PM_{10} concentrations in Belgium, Atmos. Environ., 39, 3279-3289, 2005.

Kingma, D. and Ba, J.: Adam: A method for stochastic optimization, in: Proceedings of the 3rd International Conference on Learning Representations, San Diego, USA, 3-8 May, arXiv:1412.6980v9, 2015.

Li, X., Peng, L., Yao, X., Cui, S., Hu, Y., You, C., and Chi, T.: Long short-term memory neural network for air pollutant concentration predictions: Method development and evaluation, Environ. Pollut., 231, 997-1004, 2017.

Liu, T.-H., Jeng, F.-T., Huang, H.-C., Berger, E., and Chang, J. S.: Influences of initial condition and boundary conditions on regional and urban scale Eulerian air quality transport model simulations, Chemosphere-Global Change Sci., 3, 175–183, 5   2001.

Liu, Y., Franklin, M., Kahn, R., and Koutrakis, P.: Using aerosol optical thickness to predict ground-level $PM_{2.5}$ concentrations in the St. Louis area: A comparison between MISR and MODIS, Remote Sens. Environ., 107, 33-44, 2007.

Lu, W.-Z. and Wang, W.-J.: Potential assessment of the "support vector machine" method in forecasting ambient air pollutant trends, Chemosphere, 59, 693-701, 2005.

10   Mourdoukoutas, P.: (2015, October 28), IBM To Buy The Weather Company, Forbes, Retrieved from https://www.forbes.com/.

Mahsereci, M., Ballers, L., Lassner, C., and Henning, P.: Early stopping without a validation set, arXiv:1703.09580, 2017.

Nair, V. and Hinton, G. E.: Rectified linear units improve restricted Boltzmann machines, in: Proceedings of the 27th International Conference on Machine Learning, Haifa, Israel, 21-24 June, 432, 2010.

15   Ong, B. T., Sugiura, K., and Zettsu, K.: Dynamically pre-trained deep recurrent neural networks using environmental monitoring data for predicting $PM_{2.5}$, Neural Comput. Appl., 26, 1553-1566, 2016.

Park, R. S., Lee, S. S., Shin, S.–K., and Song, C. H.: Contribution of ammonium nitrate to aerosol optical depth and direct radiative forcing by aerosols over East Asia, Atmos. Chem. Phys., 14 (4), 2185-2201, 2014.

Park, R. S., Song, C. H., Han, K. M., Park, M. E., Lee, S.-S., Kim, S.-B., and Shimizu, A.: A study on the aerosol optical 20   properties over East Asia using a combination of CMAQ-simulated aerosol optical properties and remote-sensing data via a data assimilation technique, Atmos. Chem. Phys., 11, 12275-12296, 2011.

Park, M. E., Song, C. H., Park, R. S., Lee, J., Kim, J., Lee, S., Woo, J.-H., Carmichael, G. R., Eck, T. F., Holben, B. N., Lee, S.-S., Song, C. K., and Hong, Y. D., New approach to monitor transboundary particulate pollution over Northeast Asia, Atmos. Chem. Phys., 14, 659-674, 2014.

25   Reid, C. E., Jerrett, M., Petersen, M. L., Pfister, G. G., Morefield, P. E., Tager, I. B., Raffuse, S. M., and Balmes, J. R.: Spatiotemporal prediction of fine particulate matter during the 2008 Northern California wildfires using machine learning, Environ. Sci. Technol., 49, 3887–3896, 2015.

Saad, E. W., Prokhorov, D. V., Wunsch, D. C.: Comparative study of stock trend prediction using time delay, recurrent and probabilistic neural networks, IEEE Trans. Neural Netw., 9, 1456-1470, 1998.

30   Seaman, N. L.: Meteorological modeling for air-quality assessments, Atmos. Environ., 34, 2231-2259, 2000.

Shin, S, E., Jung, C, H., and Kim, Y. P.: Analysis of the measurement difference for the PM10 concentrations between Beta-ray absorption and gravimetric methods at Gosan, Aerosol Air Qual. Res., 11, 846-853, 2011.

Tang, Y., Lee, P., Tsidulko, M., Huang, H.-C., McQueen, J. T., DiMego, G. J., Emmons, L. K., Pierce, R. B., Thompson, A. M., Lin, H.-M., Kang, D., Tong, D., Yu, S., Mathur, R., Pleim, J. E., Otte, T. L., Pouliot, G., Young, J. O., Schere, K. L.,

Davidson, P. M., and Stajner, I.: The impact of chemical lateral boundary conditions on CMAQ predictions of tropospheric ozone over the continental United States, Environ. Fluid Mech., 9, 43–58, 2009.

Wang, S. X., Zhao, B., Cai, S. Y., Klimont, Z., Nielsen, C. P., Morikawa, T., Woo, J. H., Kim, Y., Fu, X., Xu, J. Y., Hao, J. M., and He, K. B.: Emission trends and mitigation options for air pollutants in East Asia, Atmos. Chem. Phys., 14, 6571–6603, 2014.

Wiedinmyer, C., Akagi, S. K., Yokelson, R. J., Emmons, L. K., Al-Saadi, J. A., Orlando, J. J., and Soja, A. J.: The Fire Inventory from NCAR (FINN): a high resolution global model to estimate the emissions from open burning, Geosci. Model Dev., 4, 625–641, 2011.

Woo, J.-H., Kim, Y., Park, R., Choi, Y., Simpson, I. J., Emmons, L. K., and Streets, D. G.: Understanding emissions in East Asia - The KORUS 2015 emissions inventory, in: Proceedings of the American Geophysical Union Fall Meeting, New Oreleans, USA, 11-15 December, A11Q-04, 2017.

Yi, J., and Prybutok, R.: A neural network model forecasting for prediction of daily maximum ozone concentration in an industrialized urban area, Environ. Pollut., 92 , 349-357, 1996.

Yu, H., Dickinson, R. E., Chin, M., Kaufman, Y. J., Holben, B. N., Geogdzhayev, I. V., and Mishchenko, M. I.: Annual cycle of global distributions of aerosol optical depth from integration of MODIS retrievals and GOCART model simulations, J. Geophys. Res., 108(D3), 4128, 2003.
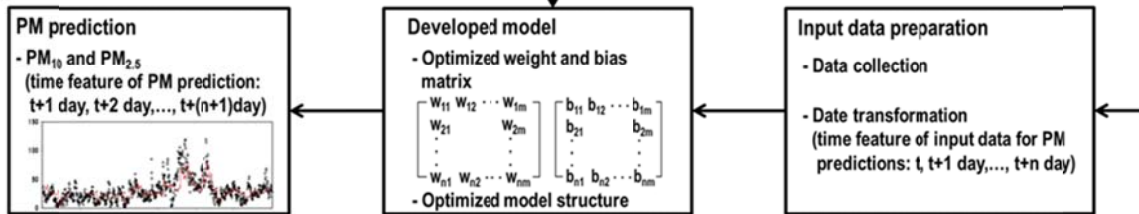
17
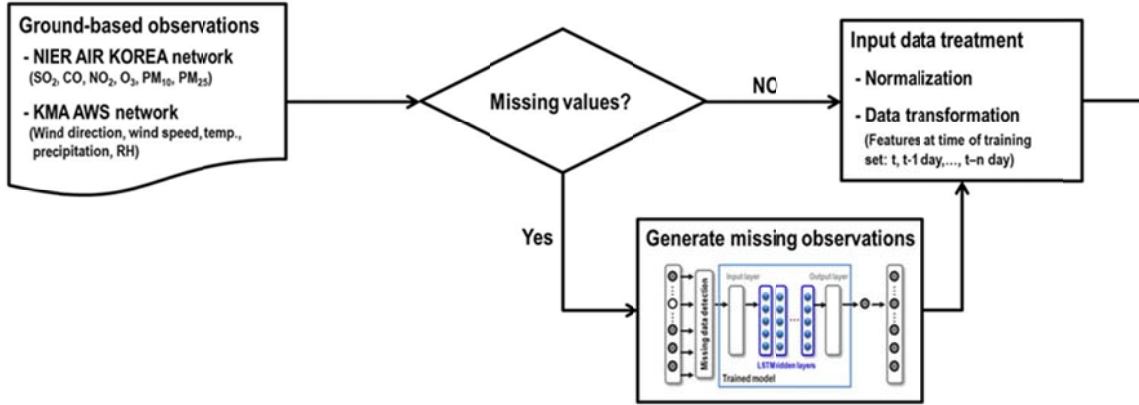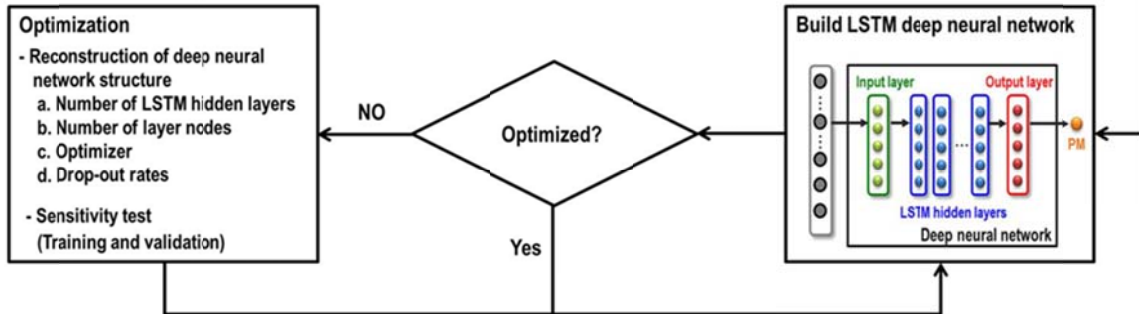
Figure 1. Schematic diagram of how the LSTM-based PM$_{10}$ and PM$_{2.5}$ prediction system was developed.
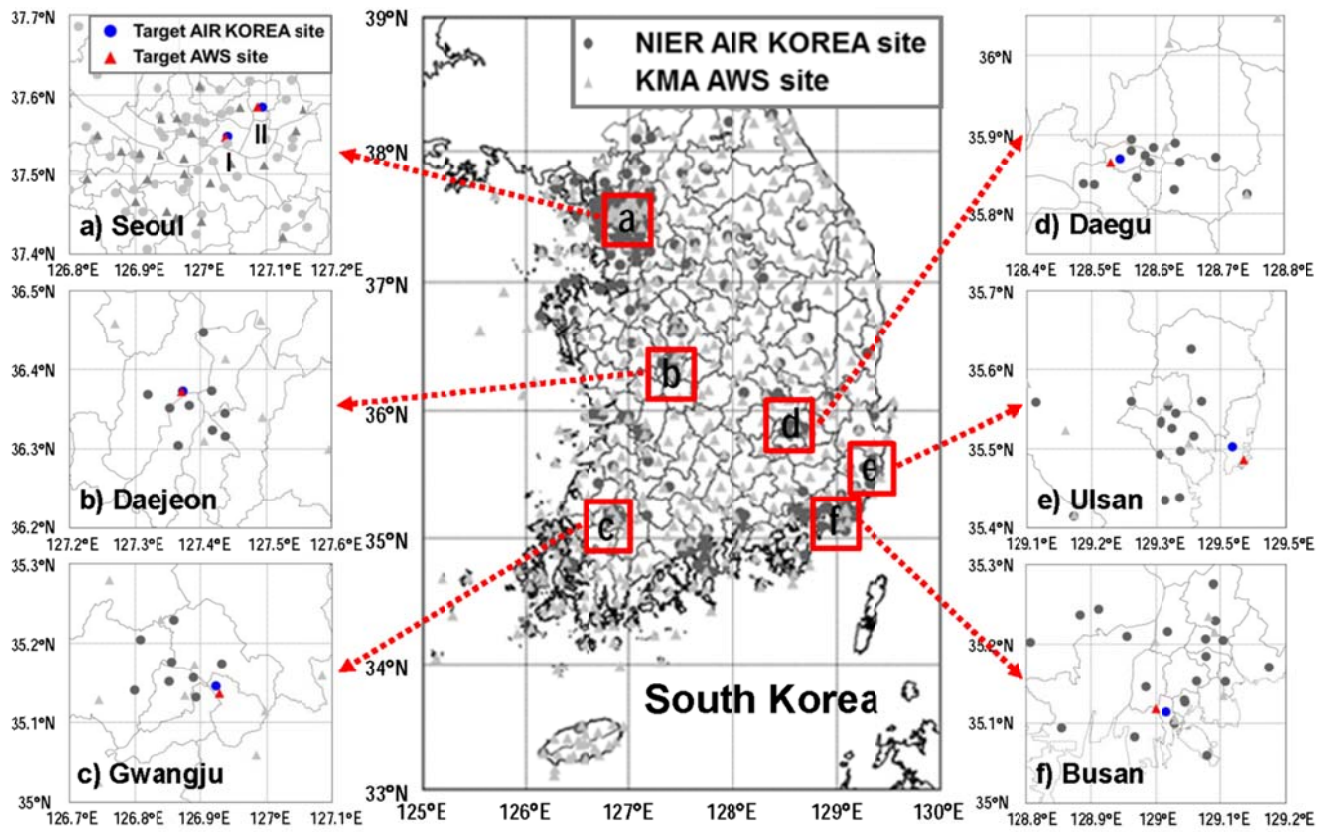
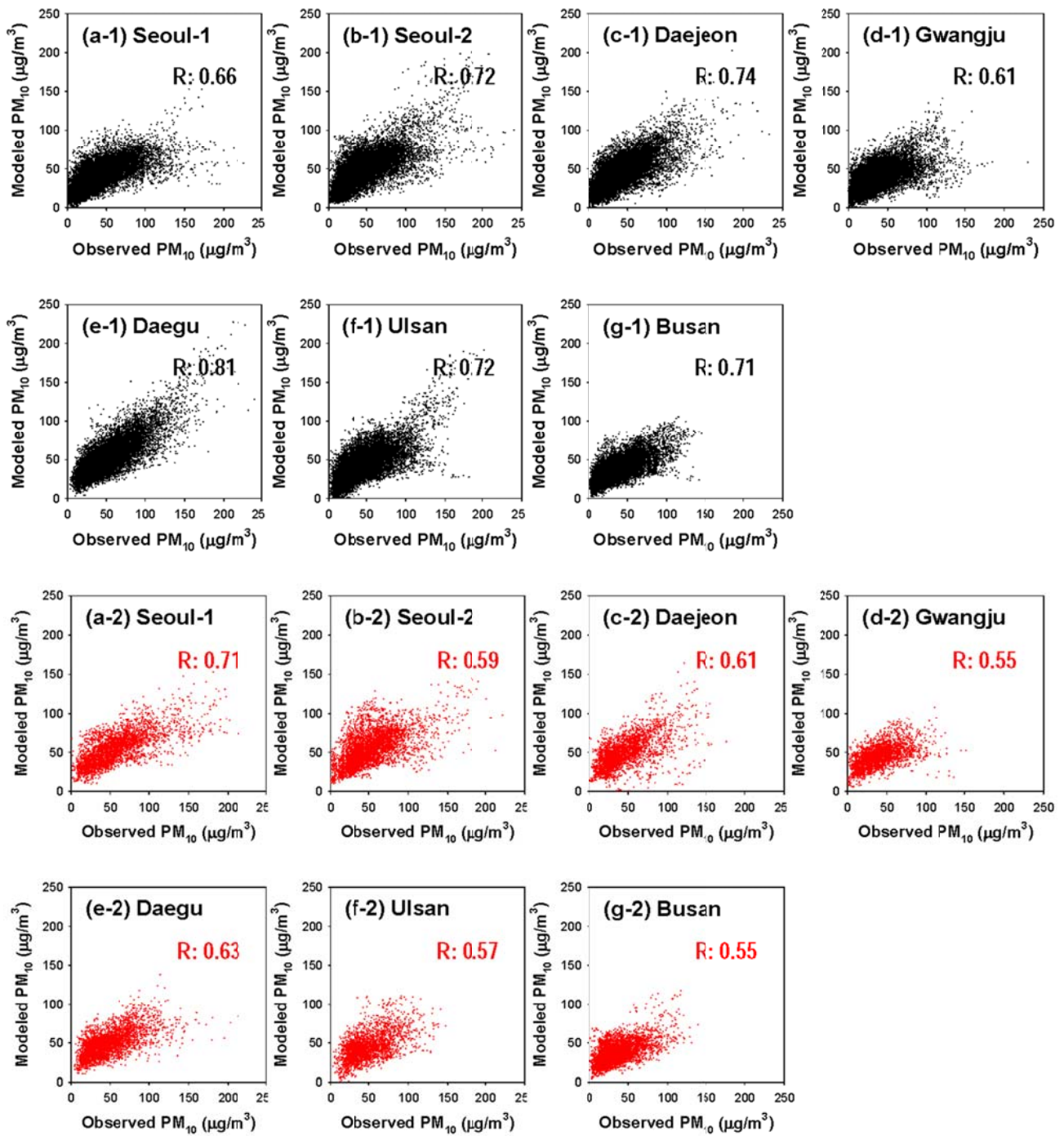**Figure 2.** Locations of NIER AIR KOREA and KMA AWS sites in South Korea.

Figure 3. Training and validating the daily PM_{10} prediction model: (a) Seoul-1; (b) Seoul-2; (c) Daejeon; (d) Gwangju; (e) Daegu; (f) Ulsan; (g) Busan. Black and red dots represent the training and validation results, respectively.
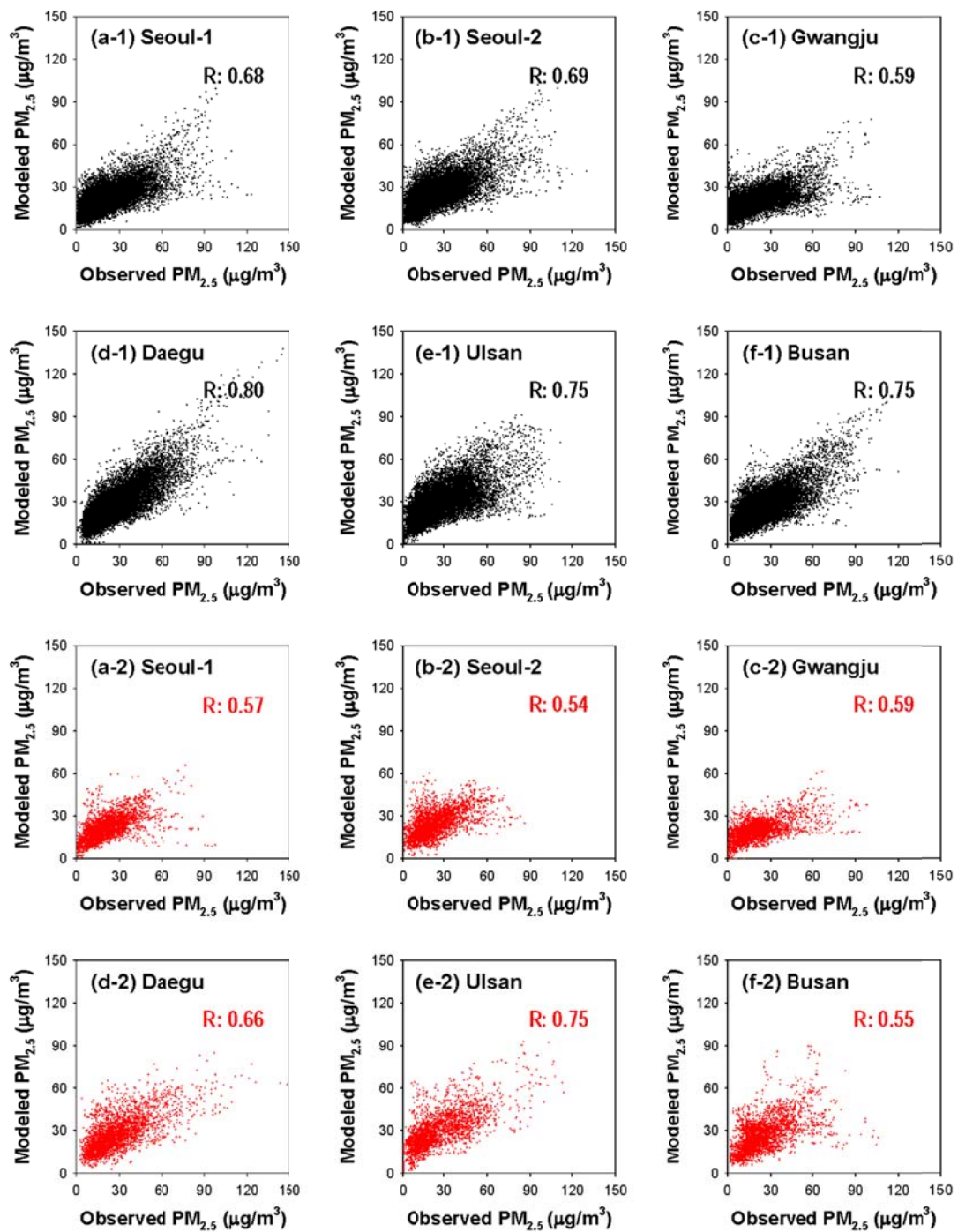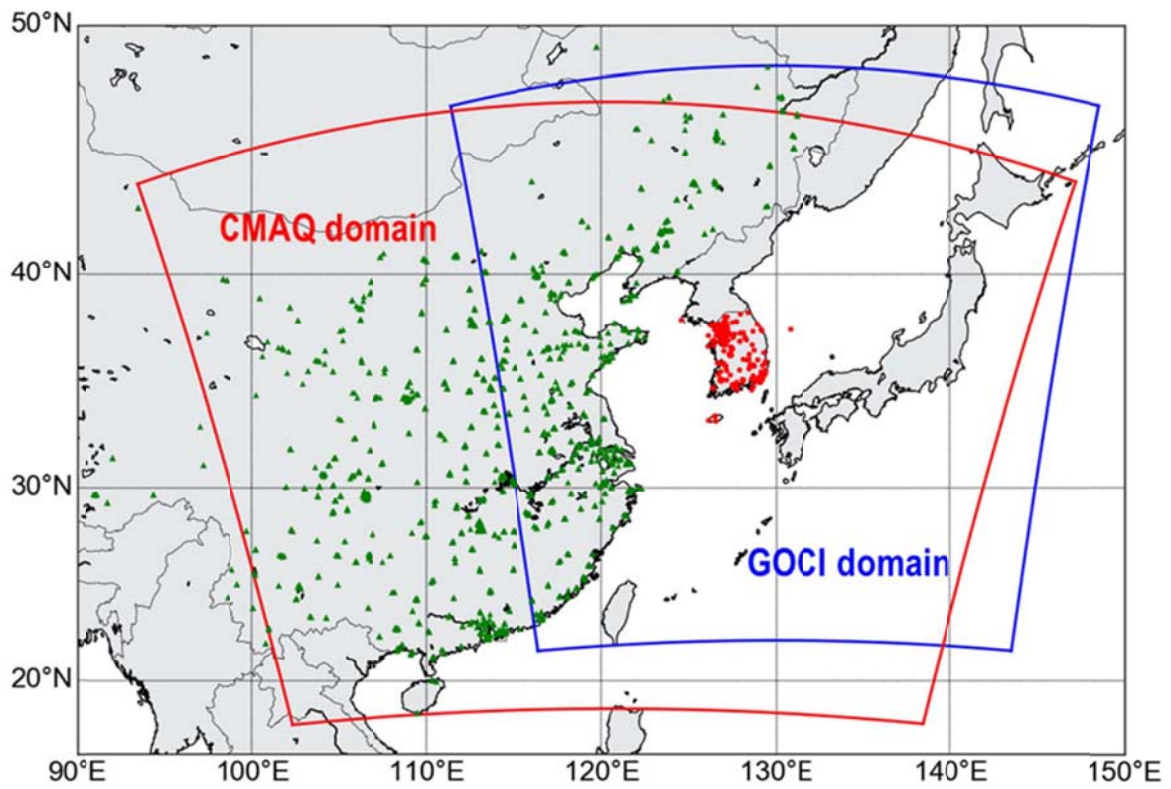
Figure 4. As Figure 3, except for PM$_{2.5}$.

Figure 5. Domains of CMAQ model simulations (red line) and GOCI sensor (blue line). Green triangles and red dots represent the locations of ground-based monitoring sites in China and South Korea, respectively.
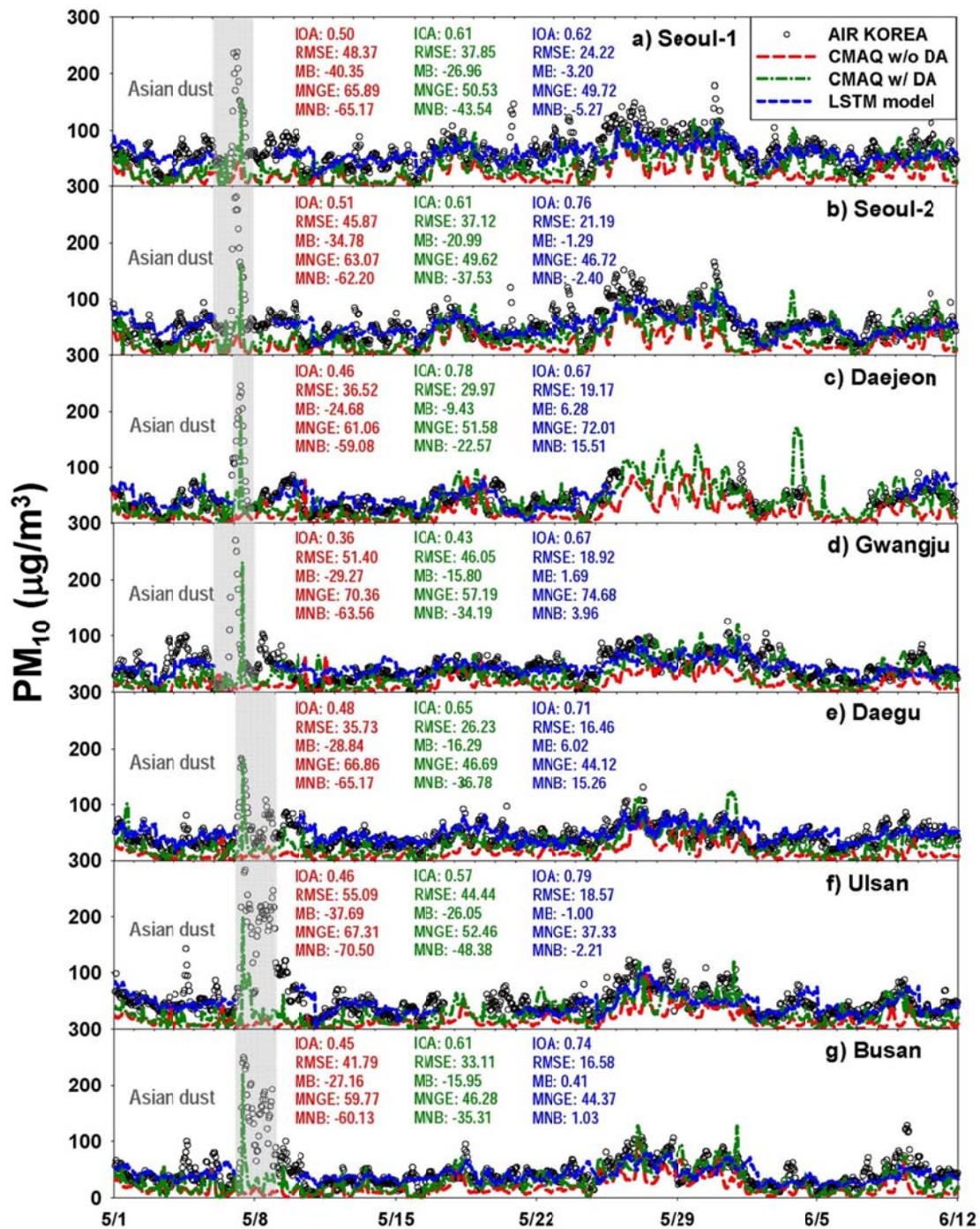
Figure 6. Comparisons between the CMAQ-calculated and LSTM-predicted and the observed PM_{10}. Black open circles show observed PM_{10} at seven sites. Green- and red-dashed lines represent CMAQ-predicted PM_{10} with and without data assimilation. Blue-dashed lines represent LSTM-predicted PM_{10}. From May 26 to June 7, the LSTM-based PM_{10} predictions at Daejeon site were not performed due to the continuous missing observations.
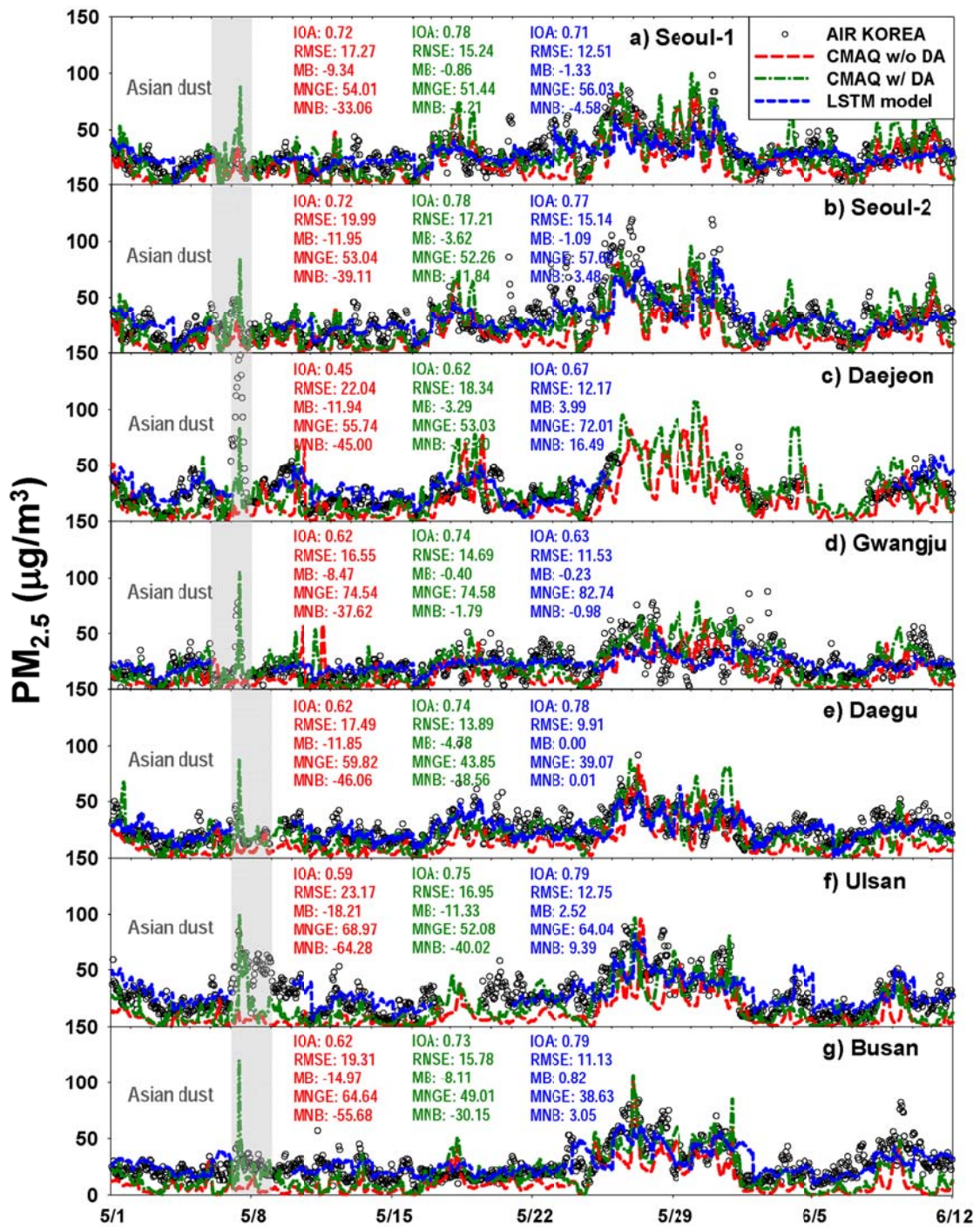
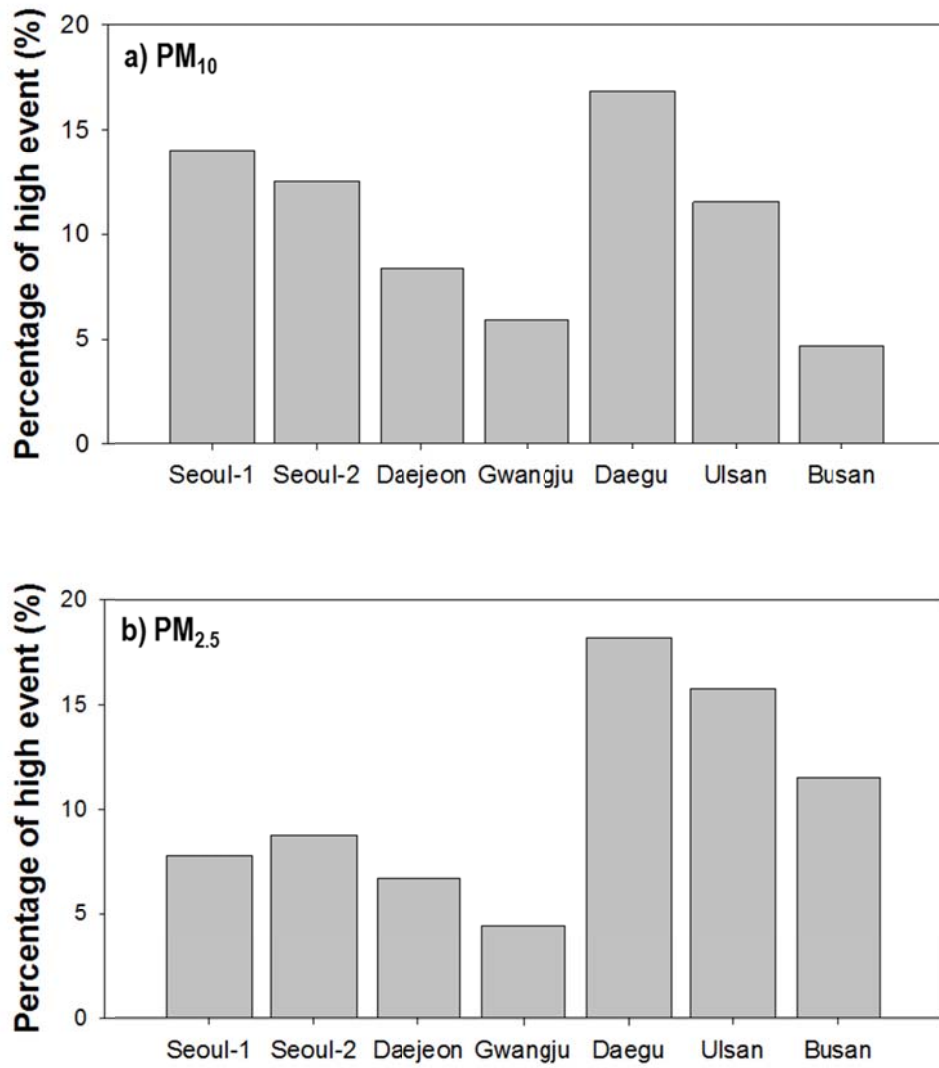**Figure 7.** As Figure 6, except for PM$_{2.5}$.

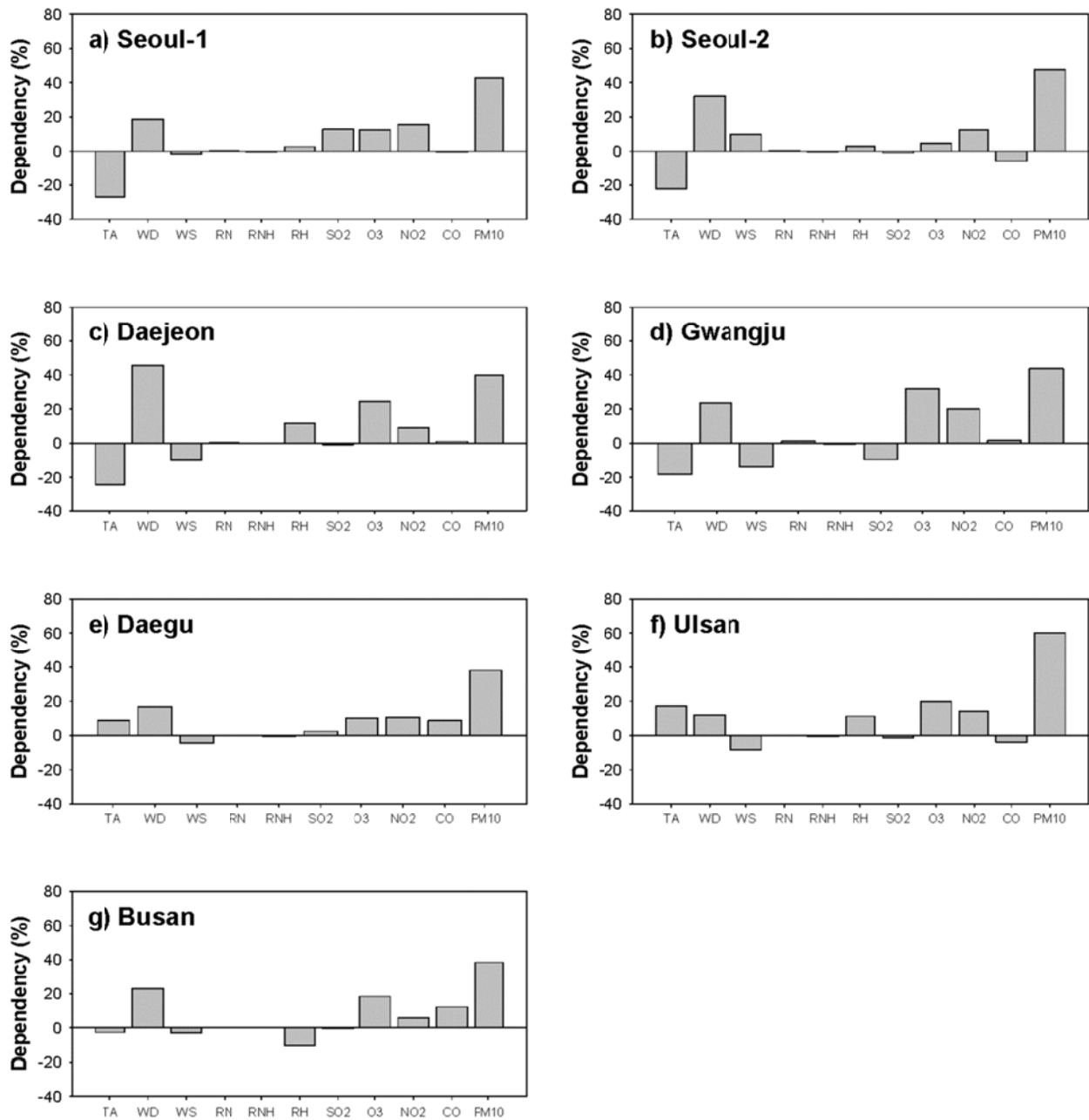**Figure 8.** Percentage (%) of high particulate matter episodes in the training data set.

Figure 9. Dependencies of input variables on the daily PM$_{10}$ predictions. TA, WD, WS, RN, RNH, and RH represent temperature, wind direction, wind speed, daily cumulative precipitation, hourly precipitation, and relative humidity, respectively. SO$_2$, O$_3$, NO$_2$, CO, PM$_{10}$, and PM$_{2.5}$ refer to the previous day's levels of these atmospheric pollutants.
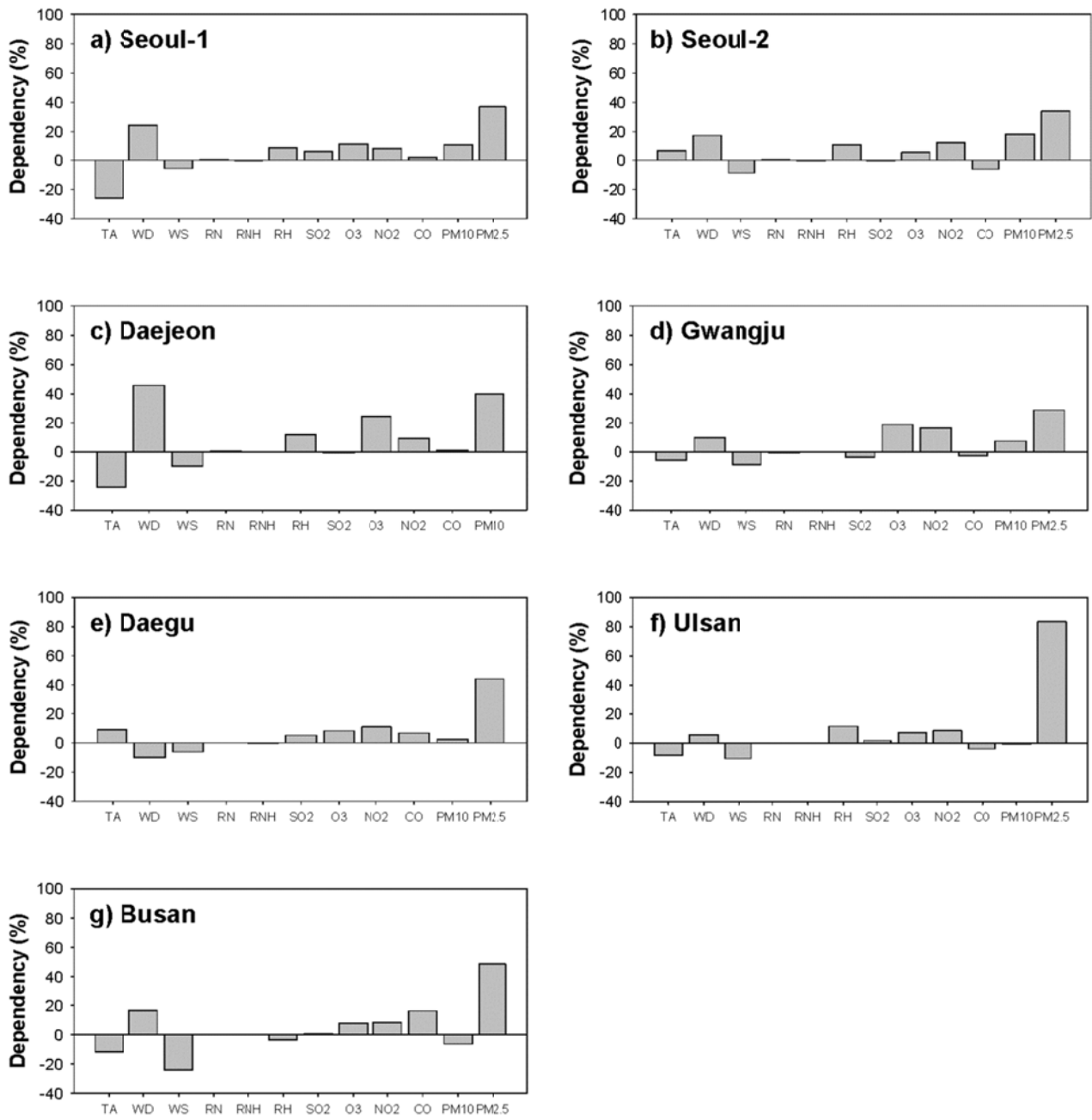
Figure 10. As Figure 9, except for PM$_{2.5}$.

Table 1. Summary of model training and validation results[1]

Species	Site	Training			Validation		
		R	MSE	RMSE	R	MSE	RMSE
PM$_{10}$	Seoul-1	0.66	379.63	19.48	0.71	589.83	24.29
	Seoul-2	0.72	347.62	18.65	0.59	551.71	23.49
	Daejeon	0.74	303.48	17.42	0.61	471.32	21.71
	Gwangju	0.61	326.98	18.08	0.55	362.88	19.05
	Daegu	0.81	259.39	16.11	0.63	378.18	19.45
	Ulsan	0.72	318.41	17.84	0.57	382.37	19.55
	Busan	0.71	230.59	15.19	0.55	394.44	19.86
PM$_{2.5}$	Seoul-1	0.68	106.73	10.33	0.57	118.24	10.87
	Seoul-2	0.69	121.07	11.00	0.54	131.36	11.46
	Daejeon	-	-	-	-	-	-
	Gwangju	0.59	112.61	10.61	0.59	151.99	12.33
	Daegu	0.80	92.32	9.61	0.66	179.67	13.40
	Ulsan	0.75	145.16	12.05	0.75	165.26	12.86
	Busan	0.75	107.63	10.37	0.55	170.53	13.06

[1] The units for MSE and RMSE are $\mu g/m^3$.

28

Table 2. Statistical analysis with modeled and observed PM$_{10}$ and PM$_{2.5}$[1]

Station	Species	Model	Statistical parameter				
			IOA	RMSE	MB	MNGE	MNB
Seoul - 1	PM$_{10}$	CMAQ w/o DA	0.50	48.37	-40.35	65.89	-65.17
		CMAQ w/ DA	0.61	37.85	-26.96	50.53	-43.54
		LSTM	0.62	24.22	-3.20	49.72	-5.27
	PM$_{2.5}$	CMAQ w/o DA	0.72	17.27	-9.34	54.01	-33.06
		CMAQ w/ DA	0.78	15.24	-0.86	51.44	-3.21
		LSTM	0.71	12.51	-1.33	56.03	-4.58
Seoul - 2	PM$_{10}$	CMAQ w/o DA	0.51	45.87	-34.78	63.07	-62.20
		CMAQ w/ DA	0.61	37.12	-20.99	49.62	-37.53
		LSTM	0.76	21.19	-1.29	46.72	-2.40
	PM$_{2.5}$	CMAQ w/o DA	0.72	19.99	-11.95	53.04	-39.11
		CMAQ w/ DA	0.78	17.21	-3.62	52.26	-11.84
		LSTM	0.77	15.14	-1.09	57.60	-3.48
Daejeon	PM$_{10}$	CMAQ w/o DA	0.46	36.52	-24.68	61.06	-59.08
		CMAQ w/ DA	0.78	26.97	-9.43	51.58	-22.57
		LSTM	0.67	19.17	6.28	72.01	15.51
	PM$_{2.5}$	CMAQ w/o DA	0.45	22.04	-11.94	55.74	-45.00
		CMAQ w/ DA	0.62	18.40	-3.29	53.03	-12.40
		LSTM	0.67	12.17	3.99	72.01	16.49
Gwangju	PM$_{10}$	CMAQ w/o DA	0.36	51.40	-29.27	70.36	-63.56
		CMAQ w/ DA	0.43	46.05	-15.80	57.19	-34.19
		LSTM	0.67	18.92	1.69	74.68	3.96
	PM$_{2.5}$	CMAQ w/o DA	0.62	16.55	-8.47	74.54	-37.62
		CMAQ w/ DA	0.74	14.69	-0.40	74.58	-1.79
		LSTM	0.63	11.53	-0.23	82.74	-0.98
Daegu	PM$_{10}$	CMAQ w/o DA	0.48	35.73	-28.84	66.86	-65.17
		CMAQ w/ DA	0.65	26.23	-16.29	46.69	-36.78
		LSTM	0.71	16.46	6.02	44.12	15.26
	PM$_{2.5}$	CMAQ w/o DA	0.62	17.49	-11.85	59.82	-46.06
		CMAQ w/ DA	0.74	13.89	-4.78	43.85	-18.56
		LSTM	0.78	9.91	0.00	39.07	0.01
Ulsan	PM$_{10}$	CMAQ w/o DA	0.46	55.09	-37.69	67.31	-70.50
		CMAQ w/ DA	0.57	44.44	-26.05	52.46	-48.38
		LSTM	0.79	18.57	-1.00	37.33	-2.21
	PM$_{2.5}$	CMAQ w/o DA	0.59	23.17	-18.21	68.97	-64.28
		CMAQ w/ DA	0.75	16.95	-11.33	52.08	-40.02
		LSTM	0.79	12.75	2.52	64.04	9.39
Busan	PM$_{10}$	CMAQ w/o DA	0.45	41.79	-27.16	59.77	-60.13
		CMAQ w/ DA	0.61	33.11	-15.95	46.28	-35.31
		LSTM	0.74	16.58	0.41	44.37	1.03
	PM$_{2.5}$	CMAQ w/o DA	0.62	19.31	-14.97	64.64	-55.68
		CMAQ w/ DA	0.73	15.78	-8.11	49.01	-30.15
		LSTM	0.79	11.13	0.82	38.63	3.05

[1] The units for RMSE and MB are μg/m^3, and those for MNGE and MNB are in %.